

Tomography is necessary for universal entanglement detection with single-copy observables

Dawei Lu,^{1,*} Tao Xin,^{1,2,*} Nengkun Yu,^{1,3,*} Zhengfeng Ji,^{1,4} Jianxin Chen,⁵ Guilu Long,² Jonathan Baugh,¹ Xinhua Peng,⁶ Bei Zeng,^{1,3,7,†} and Raymond Laflamme^{1,7,8}

¹*Institute for Quantum Computing, University of Waterloo, Waterloo N2L 3G1, Ontario, Canada*

²*State Key Laboratory of Low-Dimensional Quantum Physics and Department of Physics, Tsinghua University, Beijing 100084, China*

³*Department of Mathematics & Statistics, University of Guelph, Guelph, Ontario, Canada*

⁴*State Key Laboratory of Computer Science, Institute of Software, Chinese Academy of Sciences, Beijing, China*

⁵*Joint Center for Quantum Information and Computer Science, University of Maryland, College Park, Maryland, USA*

⁶*Hefei National Laboratory for Physical Sciences at Microscale and Department of Modern Physics, University of Science and Technology of China, Hefei, Anhui 230036, China*

⁷*Canadian Institute for Advanced Research, Toronto, Ontario, Canada*

⁸*Perimeter Institute for Theoretical Physics, Waterloo N2L 2Y5, Ontario, Canada*

Entanglement, one of the central mysteries of quantum mechanics, plays an essential role in numerous applications of quantum information theory. A natural question of both theoretical and experimental importance is whether universal entanglement detection is possible without full state tomography. In this work, we prove a no-go theorem that rules out this possibility for any non-adaptive schemes that employ single-copy measurements only. We also examine in detail a previously implemented experiment, which claimed to detect entanglement of two-qubit states via adaptive single-copy measurements without full state tomography. By performing the experiment and analyzing the data, we demonstrate that the information gathered is indeed sufficient to reconstruct the state. These results reveal a fundamental limit for single-copy measurements in entanglement detection, and provides a general framework to study the detection of other interesting properties of quantum states, such as the positivity of partial transpose and the k -symmetric extendibility.

INTRODUCTION

Entanglement is one of the central mysteries of quantum mechanics—two or more parties can be correlated in some way that is much stronger than they can be in any classical way. Famous thought experiments questioning the essence of quantum entanglement include the EPR paradox [1] and the Schrodinger’s cat [2], which ask the fundamental question whether quantum mechanics is incomplete and there are hidden variables not described in the theory. These debates about the weirdness of quantum mechanics were later put into a theorem by Bell [3], which draws a clear line between predictions of quantum mechanics and those of local hidden variable theories. Bell’s theorem was tested extensively in experiments [4–12] and quantum mechanics stands still to date.

More concretely, a bipartite quantum state ρ_{AB} of systems A and B is separable if it can be written as a mixture of product states $\rho_{AB} = \sum_i p_i \rho_A^i \otimes \rho_B^i$ with $p_i \geq 0$ and $\sum_i p_i = 1$, for some states ρ_A^i of system A and ρ_B^i of system B ; otherwise, ρ_{AB} is entangled [13]. However, not every entangled state ρ_{AB} violates Bell inequalities—some entangled states do allow local hidden variable descriptions [13].

In practice, entanglement may also be detected by measuring the ‘entanglement witnesses’, physical observables with certain values that prove the existence of quantum entanglement in a given state ρ_{AB} [14]. However, none of these entanglement witnesses could be universal. That is, the value of an entanglement witness cannot tell with certainty whether an arbitrary state is entangled or not. On the other hand, the

‘entanglement’ measures do play such a universal role. By commonly accepted axioms, the quantum state ρ_{AB} is entangled if and only if it has a nonzero value of any entanglement measure [15]. Unfortunately, entanglement measures are not physical observables.

These commonly-known restrictions on Bell inequalities, entanglement witnesses and entanglement measures raise a fundamental question: how do we universally detect entanglement through physical observables? The traditional approach to this problem is to completely characterize the quantum state by means of state tomography [16–18], a method that provides complete information of the state including, of course, entanglement measures of the state. However, performing quantum state tomography requires a large number of measurements, a daunting task for growing system sizes.

A natural idea is to find a way to obtain the value of an entanglement measure without FST. In fact, there have been a lot of efforts along this line over the past decade [19–32]. However, common techniques to achieve this purpose rely heavily on collective measurements on many identical copies of the state ρ_{AB} . That is, joint measurement on more than one copy of the state ($\rho_{AB}^{\otimes r}$ for some integer $r > 1$) is needed. This is bad news for experimentalists, as collective measurements are usually much more difficult to implement than measuring single-copy observables. It is then highly desirable to find a method that detects entanglement without FST by measuring only single-copy observables. The seeking of such a method has been pursued in recent years with both theoretical simulations and experimental realizations, leading to positive signs of realizing such an appealing task [33, 34].

In this work, we examine the possibility of detecting entanglement without FST by measuring only single-copy observables. Surprisingly, despite the previous signs, we find

* These authors contributed equally to this work.

† zengb@uoguelph.ca

that this appealing task is unfortunately impossible, if only single-copy observables are measured. That is, there is no way to determine with certainty of any entanglement measure, or even to determine whether the value is zero or not, without FST. To be more precise, this means that for any set of informationally-incomplete measurements, there always exists two different states, an entangled ρ_{AB} and a separable σ_{AB} , giving the same measurement results under this measurement. This sounds very counter-intuitive at the first sight, as entanglement is just a single value, while quantum state tomography requires measuring a set of observables that are informationally-complete, scaling as the squared dimension of the Hilbert space of the system.

Our observation is that universal detection of any property without FST enforces strong geometrical structural conditions on the set of states having that property. The set of separable states does not satisfy such conditions due to its nonlinear nature and, therefore, universal detection of entanglement without FST using single-copy measurements is not possible. There is a nice geometric picture of this fact: unless the shape of the separable states is ‘cylinder-like’, it is not possible to find a projection of the state space to a lower dimensional hyperplane with non-overlapping image for the set of separable states and entangled states.

If one allows adaptive measurements (the observable to be measured can depend on previous measurement results), a protocol was implemented in [33], claiming to have detected entanglement of a two-qubit state ρ_{AB} via single-copy measurements without FST. The protocol involves local filters that require repeated tomography on each single qubit, which leads to a bound on the entanglement measure concurrence [35] of ρ_{AB} , in case the single-qubit reduced density matrices ρ_A and ρ_B are not maximally mixed.

We design an experiment to implement this adaptive protocol as proposed in [33], and show that for certain ρ_{AB} , given the experimental data collected, the state ρ_{AB} is already completely determined. In other words, once the concurrence of ρ_{AB} is determined, the protocol already leads to a FST of ρ_{AB} , i.e. the protocol does not lead to the universal detection of entanglement without FST. This supplements our no-go result with non-adaptive measurements.

Additionally, it is worthy emphasizing that to our best knowledge this is the first experimental realization of quantum filters (or equivalently, the amplitude-damping channel) via the ancilla-assisted approach. Compared to the optical platform which does not demand extra ancilla qubits to realize an amplitude damping channel [33, 36, 37], our approach is more general and can be extended to other systems straightforwardly.

We further show that, however, if one allows joint measurements on r -copies (i.e. $\rho_{AB}^{\otimes r}$) even for $r = 2$, one can indeed find protocols that detects the entanglement of ρ_{AB} without FST. Therefore our no-go result reveals a fundamental limit for single-copy measurements, and provides a general framework to study the detection of other interesting quantities for a bipartite quantum state, such as the positivity of partial transpose [38] and k -symmetric extendibility [39].

RESULTS

We discuss a no-go result stating that it is impossible to determine universally whether a state is entangled or not without FST, with only single-copy measurements. We first prove a no-go theorem for non-adaptive measurements, and then examine the protocol with adaptive measurements as proposed in [33] in detail. We design an experiment to implement this adaptive protocol, and demonstrate that the information gathered is indeed sufficient to reconstruct the state.

Non-adaptive measurement. For any given bipartite state ρ_{AB} , one is only allowed to measure physical observables on one copy of this given state. That is, we can only measure Hermitian operators S_k that are acting on $\mathcal{H}_A \otimes \mathcal{H}_B$. For simplicity, we consider the case where both A, B are qubits. Our method naturally extends to the general case of any bipartite systems (see the Supplementary Information for details).

Now we consider a two-qubit state ρ_{AB} . In order to obtain some information about ρ , we measure a set \mathcal{S} of physical observables $\mathcal{S} = \{S_1, S_2, \dots, S_k\}$. An informationally-complete set of observables contains $k = 15$ linearly independent S_i 's. A simple choice of \mathcal{S} is the set of all two-qubit Pauli matrices other than the identity, i.e. $\mathcal{S} = \{\sigma_i \otimes \sigma_j\}$ with $i, j = 0, 1, 2, 3$, where $\sigma_0 = I, \sigma_1 = X, \sigma_2 = Y, \sigma_3 = Z$ and $(i, j) \neq (0, 0)$.

Assume that we can decide universally whether an arbitrary ρ_{AB} is entangled or not, without measuring an informationally-complete set of observables. That is, there exists a set \mathcal{S} of at most $k = 14$ physical observables such that, by measuring \mathcal{S} , we can tell for sure whether ρ_{AB} is entangled or not. For our purpose, it suffices to assume $k = 14$.

The set of all two-qubit state ρ_{AB} , denoted as \mathcal{A} , is characterized by 15 real parameters, forming a convex set in \mathbb{R}^{15} . The separable two-qubit states \mathcal{S} form a convex subset of \mathcal{A} . It is well-known that \mathcal{S} has a non-vanishing volume [40]. Denote the set of entangled states by \mathcal{E} , i.e., $\mathcal{E} = \mathcal{A} \setminus \mathcal{S}$.

The set of measurements \mathcal{S} with $k = 14$ can be visualized as the definition of projections of \mathcal{A} (hence also \mathcal{S}) onto a 14-dimensional hyperplane. If the measurement of observables in \mathcal{S} can tell for sure whether ρ_{AB} is entangled or not, the images on the hyperplane of the separable states \mathcal{S} and the entangled states \mathcal{E} must have no overlap. We illustrate this geometric idea in Fig. 1.

In fact, the only possibility to separate any set from the rest of the states without FST is that the set is an intersection of the set of all states (i.e. set \mathcal{A} as in Fig. 1) with a generalized cylinder (i.e. a set of the form $\Omega \times (-\infty, +\infty)$, where Ω is a convex set of dimension 14), In this sense, we call these sets ‘cylinder-like’, where the corresponding states can be separated from the rest of states from some 14 (or lower) dimensional projection.

Hence, to show that entanglement detection without tomography is impossible, it suffices to prove that \mathcal{S} is not ‘cylinder-like’ (in \mathbb{R}^{15}). To do this, we show that for any projection onto a 14-dimensional hyperplane with normal direction R , there always exists a two-qubit state ρ that is on the boundary of the set \mathcal{S} , such that $\rho + tR$ is entangled for some t (see Supplementary Information for details). That is, ρ and $\rho + tR$

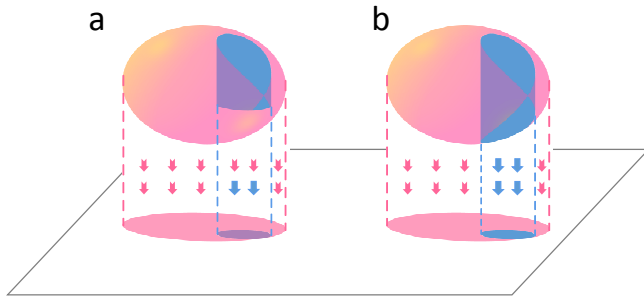


Figure 1. **Geometry of separable and entangled states.** The top pink oval represents the set of all states, denoted by \mathcal{A} . Figure (b) shows a set (indicated by blue) that is an intersection of a generalized cylinder with \mathcal{A} (i.e. ‘cylinder-like’). The projection onto the plane that is orthogonal to the boundary lines of the cylinder separates this set with the rest of the states. Figure (a) has a set (indicated by blue) inside \mathcal{A} which is not ‘cylinder-like’. Hence in fact no projection onto any plane exists that can separate the set with the rest states. The bottom ovals are the images of the top sets onto a plane, which clear show a separation of the images of the blue set from the pink set in Figure (b), but an overlap of images in Figure (a).

have the same image on the 14-dimensional hyperplane.

This geometric picture leads to a general framework to study the detection of other interesting quantities for a bipartite quantum state with single-copy measurements. Indeed, our proof also showed that the sets of states with positive partial transpose (PPT) is not ‘cylinder-like’, hence cannot be universally detected by single-copy measurements without full state tomography. With a similar method, we can show that the sets of states allowing k -symmetric extension are also not ‘cylinder like’, even for two-qubit system. This reveals a fundamental limit of single-copy measurements, that is, full state tomography is essentially needed to universally detect many non-trivial properties of quantum states (e.g., separability, PPT, k -symmetric extendability, see Supplementary Information for details).

Adaptive measurement. In case of adaptive protocols, the observable to be measured in each step can depend on previous measurement results. This kind of measurement protocol can be formulated as follows. First an observable H_1 is chosen, and $\text{tr}(H_1\rho)$ is measured. Suppose the measurement result is α_1 . Based on α_1 , observable H_{2,α_1} is chosen, and $\text{tr}(H_{2,\alpha_1}\rho)$ is measured. Suppose the measurement result is α_2 . Based on α_1, α_2 , observable H_{3,α_1,α_2} is chosen, $\text{tr}(H_{3,\alpha_1,\alpha_2}\rho)$ is measured and so on.

The protocol in [33] to determine the concurrence [35] of a two-qubit state without FST falls into the category of adaptive measurements. We implement this protocol and show that given the experimental data collected for certain state ρ_{AB} , this protocol in fact leads to FST of ρ_{AB} . That is, this protocol does not lead to universal detection of entanglement without FST.

First let us briefly introduce the idea of entanglement distillation via an iteratively filtering procedure [33] depicted in Fig. 2a. For an unknown two-qubit state ρ_{AB}^0 , we measure the local reduced density matrices $\rho_A^0 = \text{tr}_B(\rho_{AB}^0)$ and $\rho_B^0 = \text{tr}_A(\rho_{AB}^0)$ for both qubits. In case ρ_A^0 and ρ_B^0 are not

fully mixed, we design the first filter $\mathcal{F}_A^0 = 1/\sqrt{2\rho_A^0}$ based on the information of ρ_A^0 , and evolve ρ_{AB}^0 to ρ_{AB}^1 by applying \mathcal{F}_A^0 . Similarly, the same procedure is repeated for qubit B. The iterative applications of filters are kept on going, and at step k , the reduced density matrices of the qubits will be ρ_A^k and ρ_B^k .

In case both ρ_A^0 and ρ_B^0 are not identity, the iterative procedure described above leads to a ‘distillation’ of the density matrices ρ_A^k and ρ_B^k and it is guaranteed that they both converge to identity eventually [41]. All of the reduced density matrices ρ_A^i and ρ_B^i ($i = 0, 1, \dots, k$) are recorded during the iterative procedure. At step k , when ρ_A^k and ρ_B^k are sufficient close to identity, they can be used to reconstruct a bound on the value of entanglement in ρ_{AB}^0 through the optimal witness $W(\rho_{AB}^0)$ that is only dependent on ρ_A^i and ρ_B^i ($i = 0, 1, \dots, k$) (up to local unitary transformations), whose value hence tells whether ρ_{AB}^0 is entangled or not [33].

At the first sight, the above procedure seems feasible to determine the value of entanglement without FST, since only single-qubit density matrices ρ_A^i and ρ_B^i ($i = 0, 1, \dots, k$) are repeatedly measured and only local unitary transformations are used in constructing the optimal witness. That is, it seems that the two-qubit correlations in ρ_{AB}^0 are never measured, which hence not lead to FST. However, a detailed look shows it is not the case. The key observation here is that, ‘local filters’ are in fact ‘weak’ measurements that do record the correlations in ρ_{AB}^0 . This is because that the filters cannot be implemented with probability one, so the correlation in ρ_{AB}^0 is ‘encoded’ in the information that all the filters are implemented successfully. In other words, what these local filters and local tomography on each single qubit does, is in fact an FST of ρ_{AB}^0 .

In order to demonstrate the relationship between the local filters and FST, we simulate the local filter procedure by choosing different number of applied filters as depicted in Fig. 2a. It turns out, in many case $k = 4$ (five filters) is enough to uniquely determine ρ_{AB}^0 based on the data of ρ_A^i and ρ_B^i ($i = 0, 1, \dots, k$). Thus, the information of ρ_A^i and ρ_B^i lead to an FST of ρ_{AB}^0 .

As an example, we illustrate the simulation with the input state chosen as equation (5) with $\lambda = 0.2$, and the result is shown in Fig. 2b. Initially, we have 15 real parameters (i.e. degrees of freedom, DOF for short) to determine ρ_{AB}^0 (ignoring the identity part due to the normalization condition). When more and more filters are applied, DOF is decreasing eventually since we are acquiring more and more knowledge about the original input state. For example, the initial local reduced density matrices ρ_A^0 and ρ_B^0 before applying any filter can already reduce DOF to 9; ρ_B^1 after the first filter provides three more constraints so DOF lowers to 6, and so on. It is found that with 5 filters, the input state ρ_{AB}^0 can be uniquely determined via the collected information of the reduced density matrices. And this procedure works similarly for many other two-qubit state ρ_{AB}^0 , where 5 filters are found to be enough to reconstruct ρ_{AB}^0 , as we will show in our experiment results.

Experimental protocol in NMR setup. To experimentally implement the protocol as presented in Fig. 2a, we first discuss how to realize the local filters in NMR system. Without

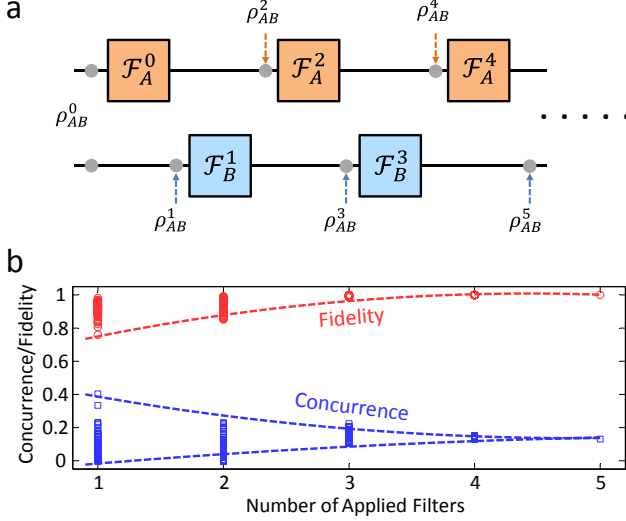


Figure 2. **Circuit and simulation results of the theoretical protocol.** (a) Schematic circuit for implementing the filter-based entanglement distillation proposal for an unknown two-qubit state ρ_{AB}^0 . $\mathcal{F}_{A,B}^i = 1/\sqrt{2\rho_{A,B}^i}$ ($i \geq 0$) is the i th local filter applied on A or B, where $\rho_A^i = \text{tr}_B(\rho_{AB}^i)$ and $\rho_B^i = \text{tr}_A(\rho_{AB}^i)$ are the local reduced density matrices of the current two-qubit state ρ_{AB}^i . The gray dots mean a single-qubit tomography is implemented at that place. (b) Simulated variation of concurrence and fidelity as the increase number $1 \leq m \leq 5$ of applied filters. The simulated state is chosen as equation (5) with $\lambda = 0.2$. For any given m , we collected all the available reduced density matrices at this stage and reconstructed 100 possible input state. When $m \leq 4$, the reconstructed state is not unique due to the lack of constraints, so both the concurrence and fidelity have some distributions. When $m = 5$, the input state can be uniquely determined, and the concurrence and fidelity converges to a single point. The dashed blue and red curves show the envelopes of the variations of concurrence and fidelity along with m , respectively.

loss of generality, we can consider a local filter \mathcal{F}_A applied on qubit A as an example. For any \mathcal{F}_A , it can always be decomposed into the form of $U_A \Lambda_A V_A$ via singular value decomposition, where U_A and V_A are single-qubit unitaries and Λ_A is a diagonal Kraus operator

$$\Lambda_A = \begin{pmatrix} 1 & 0 \\ 0 & \sqrt{1-\gamma_A} \end{pmatrix}. \quad (1)$$

$\gamma_A \in [0, 1]$ relies on \mathcal{F}_A and indicates the probability that the excited state $|1\rangle$ decays to the ground state $|0\rangle$ when a system undergoes Λ_A . Although non-unitary, Λ_A can be expanded to a two-qubit unitary with the aid of an ancilla qubit 1. Basically, if a two-qubit unitary can transform

$$\begin{aligned} |0\rangle_1|0\rangle_A &\rightarrow |0\rangle_1|0\rangle_A, \\ |0\rangle_1|1\rangle_A &\rightarrow \sqrt{1-\gamma_A}|0\rangle_1|1\rangle_A + \sqrt{\gamma_A}|1\rangle_1|1\rangle_A, \end{aligned} \quad (2)$$

the quantum channel on the system qubit A would be Λ_A by post-selecting the subspace in which the ancilla qubit 1 is $|0\rangle$. One possible unitary transformation that satisfies equation (2)

is

$$\mathcal{U}_{1A} = \begin{pmatrix} 1 & 0 & 0 & 0 \\ 0 & \sqrt{1-\gamma_A} & 0 & \sqrt{\gamma_A} \\ 0 & 0 & 1 & 0 \\ 0 & -\sqrt{\gamma_A} & 0 & \sqrt{1-\gamma_A} \end{pmatrix}. \quad (3)$$

The operation \mathcal{U}_{1A} is thus a controlled rotation: when the system qubit A is $|0\rangle$, the ancilla remains invariant; when A is $|1\rangle$, the ancilla undergoes a rotation $R_{-y}(\theta_A) = e^{i\theta_A\sigma_y/2}$ where $\theta_A = 2\arccos\sqrt{1-\gamma_A}$. Therefore, in an ancilla-assisted system with the ancilla initialized to $|0\rangle$, the local filter \mathcal{F}_A can be accomplished through a two-qubit unitary gate $(I \otimes U_A)\mathcal{U}_{1A}(I \otimes V_A)$ followed by post-selecting the subspace in which ancilla is $|0\rangle$.

NMR implementation. To implement the aforementioned filter-based entanglement distillation protocol as presented in Fig. 2a in NMR, we need a 4-qubit quantum processor consisting of two system qubits A and B, and two ancilla qubits 1 and 2. Our 4-qubit sample is ^{13}C -labeled trans-crotonic acid dissolved in d6-acetone. The structure of the molecule is shown in Fig. 3, where C_1 to C_4 denote the four qubits. The methyl group M, H_1 and H_2 were decoupled throughout all experiments. The internal Hamiltonian of this system can be described as

$$\mathcal{H}_{int} = \sum_{j=1}^4 \pi\nu_j\sigma_z^j + \sum_{j<k,=1}^4 \frac{\pi}{2} J_{jk}\sigma_z^j\sigma_z^k, \quad (4)$$

where ν_j is the chemical shift of the j th spin and J_{jk} is the J-coupling strength between spins j and k . We assigned C_3 and C_2 as system qubits A and B, and C_4 and C_1 as ancilla qubits 1 and 2 to assist in mimicking the filters, respectively. All experiments were conducted on a Bruker DRX 700MHz spectrometer at room temperature.

Our target input state was chosen as a mixed state involving one Bell-state portion and two product-state portions, with the weight of Bell-state portion tunable. The state is written as

$$\rho_{AB}^0 = \lambda|\phi_B\rangle\langle\phi_B| + (1-\lambda)(|\phi_1\rangle\langle\phi_1| + |\phi_2\rangle\langle\phi_2|)/2, \quad (5)$$

where

$$\begin{aligned} |\phi_B\rangle &= (|00\rangle + |11\rangle)/\sqrt{2}, \\ |\phi_1\rangle &= (|0\rangle - i|1\rangle)(|0\rangle + |1\rangle)/2, \\ |\phi_2\rangle &= (|0\rangle + |1\rangle)(|0\rangle - 2i|1\rangle)/\sqrt{10} \end{aligned} \quad (6)$$

have concurrences 1, 0 and 0, respectively. The parameter λ in $[0, 1]$ is thus proportional to the value of entanglement of ρ_{AB}^0 . In experiment, we varied λ from 0.2 to 0.7 with step size 0.1 for every point, and implemented the proposal correspondingly. Considering the two ancilla, the overall input state for our 4-qubit system is thus $|0\rangle\langle 0| \otimes \rho_{AB}^0 \otimes |0\rangle\langle 0|$. As shown in Fig. 4, we prepared a pseudo-pure state from the thermal equilibrium via spatial average technique [42–44] and then created three components $|\phi_B\rangle$, $|\phi_1\rangle$ and $|\phi_2\rangle$ on the

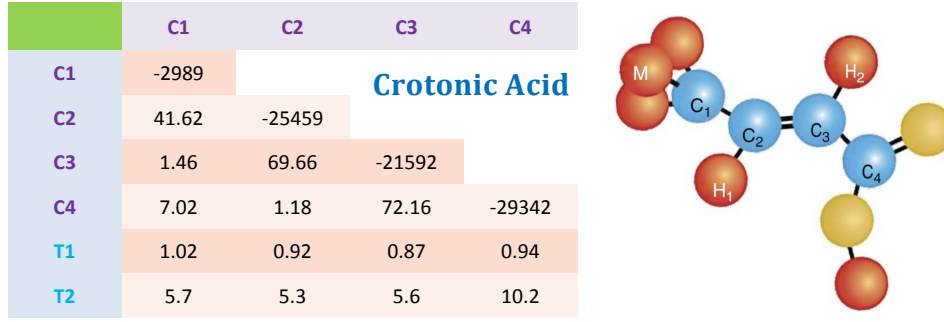


Figure 3. **Molecular structure and Hamiltonian parameters of ^{13}C -labeled trans-crotonic acid.** C_1 , C_2 , C_3 and C_4 are used as four qubits in the experiment, and M , H_1 and H_2 are decoupled throughout the experiment. In the table, the chemical shifts with respect to the Larmor frequency 176.05MHz and J-coupling constants (in Hz) are listed by the diagonal and off-diagonal numbers, respectively. The relaxation time scales T_1 and T_2 (in Seconds) are shown at bottom.

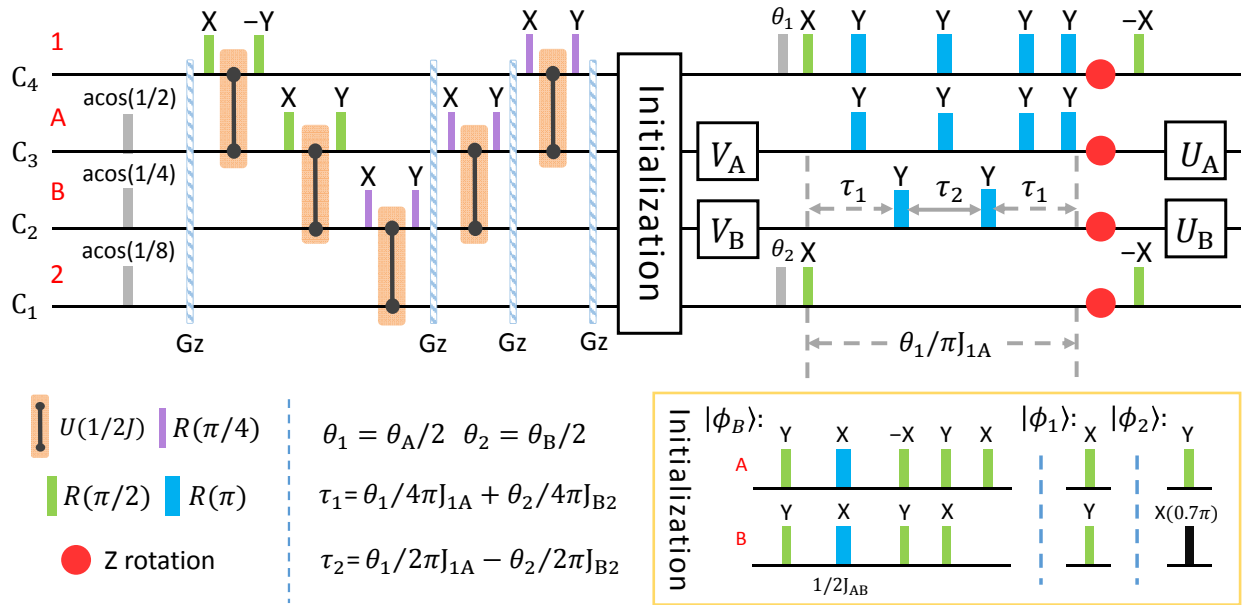


Figure 4. **NMR sequence to realize the filter-based proposal of entanglement distillation.** In particular, this sequence displays how to realize the first two filters \mathcal{F}_A^0 and \mathcal{F}_B^1 in terms of NMR pulses. All other sequences can be obtained analogously. A (marked by C_3) and B (marked by C_2) are system qubits to implement the proposal, while qubit 1 (marked by C_4) and 2 (marked by C_1) are ancilla qubits to assist in mimicking the filters. First the 4-qubit system is prepared to the PPS by spatial average technique which is shown before the initialization step. Then the system qubits are initialized to $|\phi_B\rangle$, $|\phi_1\rangle$ and $|\phi_2\rangle$ via three independent experiments illustrated in the lower-right inset, respectively. The part after the initialization step is the sequence for realizing filters. V_A , V_B , U_A , U_B , θ_1 and θ_2 all depend on the measured results of reduced density matrices. Refer to the main text for detailed information of the parameters.

system qubits, respectively (see Methods for detailed descriptions). Subsequently, each component undergoes the whole filtering and single-qubit readout stage, with the final result obtained by summarizing over all three experiments.

A two-qubit state tomography was implemented on the system qubits after creating ρ_{AB}^0 . ρ_0^e was reconstructed in experiment and its fidelity compared with the expected ρ_{AB}^0 is over 98.2% for any λ (Supplementary Table S1). This two-qubit state tomography is not required in the original proposal [33] in which only single-qubit measurements are necessary. However, since we claim that the filter-based proposal has already provided sufficient information to reconstruct the initial two-qubit state ρ_0^e , we need to compare it with ρ_f^e which is

constructed after running the entire proposal. To support our viewpoint, we have to show that ρ_0^e and ρ_f^e are the same up to minor experimental errors. This comparison is the only purpose of doing a two-qubit state tomography here.

Now we show how to realize local filtering operations in NMR. By measuring the local reduced density matrix ρ_A^0 of the input state ρ_{AB}^0 , the first filter in Fig. 2a was calculated via $\mathcal{F}_A^0 = 1/\sqrt{2\rho_A^0}$ and decomposed into $U_A^0\Lambda_A^0V_A^0$. Since U_A^0 and V_A^0 are merely local unitaries on qubit A, they can be realized by local radio-frequency (RF) pulses straightforwardly. Λ_A^0 , which can be expanded to a 2-qubit controlled rotation \mathcal{U}_{1A}^0 (see equation (3)) in a larger Hilbert space, was performed by a combination of local RF pulses and J-coupling

evolutions[45]

$$\mathcal{U}_{1A} = R_{-x}^1(\pi/2)U(\theta_A/2\pi J_{1A})R_x^1(\pi/2)R_{-y}^1(\theta_A/2), \quad (7)$$

where $U(\theta_A/2\pi J_{1A})$ represents the J-coupling evolution $e^{-i\theta_A\sigma_z^1\sigma_z^A/4}$ between qubit 1 and A, and $\theta_A = 2\arccos\sqrt{1-\gamma_A}$ depends on Λ_A^0 . After this filter, the system evolved to ρ_{AB}^1 and a single-qubit tomography on qubit B was implemented, as shown by the gray dots in Fig. 2a. The same procedure was repeated for qubit B to realize the second filter $\mathcal{F}_B^1 = 1/\sqrt{2}\rho_B^1$. In experiment, these two filters \mathcal{F}_A^0 and \mathcal{F}_B^1 were carried out simultaneously using the partial decoupling technique as shown in Fig. 4, with additional Z rotations in the tail to compensate the unwanted phases induced by the chemical shift evolutions. In Fig. 4, θ_1 and θ_2 pulses are used to realize $R_{-y}^1(\theta_A/2)$ and $R_{-y}^1(\theta_B/2)$, respectively, and the free evolution time τ_1 and τ_2 are defined as

$$\begin{aligned} \tau_1 &= \theta_1/4\pi J_{1A} + \theta_2/4\pi J_{B2} \\ \tau_2 &= \theta_1/2\pi J_{1A} - \theta_2/2\pi J_{B2}. \end{aligned} \quad (8)$$

Here we have assumed that $\tau_2 > 0$ ($\theta_1/2\pi J_{1A} > \theta_2/2\pi J_{B2}$). When $\tau_2 < 0$, the circuit just needs to be modified slightly by adjusting the positions of refocusing π pulses. All the other filters have analogical structures with the one shown in Fig. 4, and they were always carried out on qubit A and B simultaneously since they commute.

Every time after performing one local filter, we implemented a single-qubit tomography on the other qubit rather than the working qubit on which the filter was applied. The reason is that the working qubit has evolved to identity due to the properties of the filter. The tomographic result was used to design the next filter on the other qubit. In principle, before applying any filters, it is necessary to reset the two ancilla qubits to $|00\rangle$. As it is difficult to refresh the spins in NMR, an alternative way was adopted in our experiments. For example, to realize \mathcal{F}_A^2 , we packed it together with \mathcal{F}_A^0 and generated a new operator. It can be regarded as a 2-in-1 filter and implemented in the same way. Hence, we avoided the reset operations throughout the experiments and for any individual experiment we just started from the original two-qubit state ρ_{AB}^0 . This feedback-based filtering operations continued to be executed till five filters accomplished and seven 1-qubit tomographies carried out, as shown in Fig. 2a.

From the above discussions, we have shown that the NMR experiments only contain free J-coupling evolutions and single-qubit unitaries. See the circuit in Fig. 4. For the J-coupling evolutions, we drove the system to undergo the free Hamiltonian in equation (4) for some time. For local unitaries, we utilized GRAdient Ascent Pulse Engineering (GRAPE) techniques [46, 47] to optimize them. The GRAPE approach provided 1 ms pulse width and over 99.8% fidelity for every local unitary, and furthermore all pulses were rectified via a feedback-control setup in NMR spectrometer to minimize the discrepancies between the ideal and implemented pulses [48–50].

Experimental results and error analysis. We prepared six input states by varying λ from 0.2 to 0.7 with 0.1 step size in the form of equation (5). After the preparations, we

performed two-qubit full state tomography on each state, and reconstructed them as ρ_0^e where the superscript e means experiment. The fidelity between the theoretical state ρ_{AB}^0 and measured state ρ_0^e is over 98.2% for each of the six input states. The infidelity can be attributed to the imperfections of PPS, GRAPE pulses and minor decoherence effect. Nevertheless, this infidelity is merely used to evaluate the precision of our input state preparation. For the latter experiments, we only compared the experimental results with ρ_0^e , as ρ_0^e was the actual state from which we started the filter-based experiment.

After initial state preparation and each filter, we obtained the reduced density matrix of qubit A and/or B by single-qubit tomography in the subspace where the ancilla qubits are $|00\rangle$ (see Methods). Refer to Fig. 2a to see the seven gray dots where single-qubit tomography occurred. The average fidelity between the measured single-qubit state and the expected state computed by ρ_0^e is about 99.5% (Supplementary Table S1), which demonstrates that our filtering operations and single-qubit tomographies are accurate.

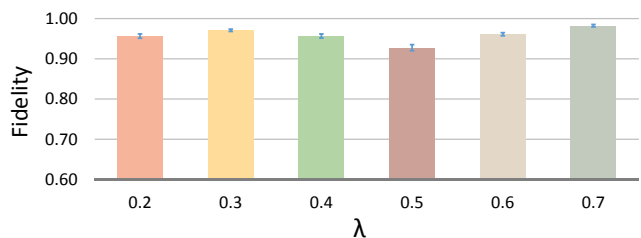


Figure 5. **Fidelities between ρ_0^e and ρ_f^e for different λ 's.** ρ_0^e is obtained from two-qubit state tomography right after the creation of the input state ρ_{AB}^0 , and ρ_f^e from the maximum likelihood reproduction of ρ_{AB}^0 based on the own seven single-qubit states. The error bar comes from the fitting uncertainty when extracting the NMR spectra into quantum states. All fidelities are over 92.0%, which means the initial two-qubit state is able to be well-reconstructed merely by the seven single-qubit states.

With the seven single-qubit states in hand, we could reproduce the initially prepared two-qubit state ρ_0^e . The maximum likelihood method was adopted here and ρ_f^e was found to be closest to the experimental raw data. Not surprisingly, ρ_f^e is very similar to ρ_0^e , and the fidelity between them for every λ is over 92.0% as illustrated in Fig. 5. Moreover, the real parts of the density matrices ρ_0^e and ρ_f^e are shown in Fig. 7. The experimental results clearly reveal that the information of the seven single-qubit states collected during the filter-based entanglement distillation procedure already enables the reproduction of the initial two-qubit state. In other words, this filter-based proposal to universally detect and distill entanglement is equivalent compared to doing a two-qubit state tomography.

Afterwards, we computed the concurrence for each case with different input two-qubit state. Concurrence is an entanglement monotone defined for a mixed state ρ of two qubits

$$C(\rho) = \max(0, \lambda_1 - \lambda_2 - \lambda_3 - \lambda_4), \quad (9)$$

where $\lambda_1, \lambda_2, \lambda_3$ and λ_4 are the eigenvalues of

$$R = \sqrt{\sqrt{\rho}(\sigma_y \otimes \sigma_y)\rho^*(\sigma_y \otimes \sigma_y)\sqrt{\rho}} \quad (10)$$

in decreasing order. Apparently, the concurrence is proportional to λ since λ is the weight of Bell-state which is the only term contributing to entanglement. In Fig. 6, the brown curve displays the value of concurrence as a monotonically increasing function of Bell-state weight λ . The blue squares represent the concurrence of ρ_0^e , the state obtained from two-qubit state tomography on the experimentally prepared state. Recall that the preparation fidelity is always over 98.2% so the blue squares do not deviate much from the brown curve. The red circles represent the concurrence of ρ_f^e , which ideally should be the same as blue squares if there are no experimental errors. However, in experiment we have inevitable errors from many factors such as the imprecision of the single-qubit readout stage, the imperfect application of filters and the relaxation, and we need to take them into account.

For convenience, we assume the errors originate from three primary aspects and they are additive. One error is caused by the imprecision of the single-qubit tomography procedure. As we used a least-square fitting algorithm to analyze the outcome spectra and converted the data into quantum states, the fitting induced about 3.00% uncertainty to the single-qubit readout result. The second is the error from applying imperfect filters in experiment. It mainly comes from the errors of accumulating GRAPE pulses, which is about 1.59% for each filter operation. The third error, to the lesser extent, is about 1.20% caused by decoherence. Therefore, in total we estimated at most 5.79% error might occur in the entire process. We dealt with it as an artificial noise and embedded it into the theoretical input state ρ_{AB}^0 . In simulation, we first discretized λ to 200 values from $\lambda = 0.1$ to $\lambda = 0.8$. For a given λ , 2500 states were randomly sampled deviated from ρ_{AB}^0 within 5.79% noise range. For every sampled state, the concurrence was calculated and projected onto one point in Fig. 6. Hence, a colored band-region was generated considering the density of points. All of our experimental results have fallen into this region, which is consistent with the simulation model.

DISCUSSION

We proved a no-go theorem that there is no way to detect entanglement for an arbitrary bipartite state ρ_{AB} without FST, if only single-copy non-adaptive measurements are allowed. Our observation is due to a nice geometric picture: unless the shape of the separable states is ‘cylinder-like’, it is not possible to find a projection of the state space to a lower dimensional hyperplane with non-overlapping image for the set of separable states and entangled states. Our method provides a general framework to study the detection of other interesting quantities for a bipartite quantum state, such as positive partial transpose and k -symmetric extendibility.

We also have investigated the case of adaptive measurements. It is proposed in [33] that the entanglement measure concurrence for two-qubit states can be determined without FST, via only single-copy measurements. To implement this protocol, we developed an ancilla-assisted approach to realize the filters. Practically, our technique can be extend to other quantum systems other than optics to implement an amplitude

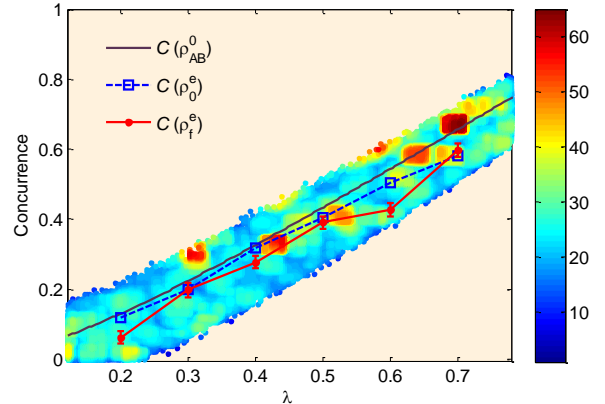


Figure 6. Concurrence of ρ_{AB}^0 , ρ_0^e , and ρ_f^e as a function of the Bell-state weight λ . The brown curve shows the concurrence computed by the theoretical state ρ_{AB}^0 , and exhibits the value of concurrence as a monotonically increasing function of λ . The blue squares represent the concurrence of ρ_0^e , the state obtained from two-qubit state tomography right after the input state preparation. Generally we can roughly assume this state is the truly prepared state, and the following filtering operations are always applied this state as long as we neglect the measurement error of reconstructing ρ_0^e . The red circles represent the concurrence of ρ_f^e , the state reproduced from the seven single-qubit states. Ideally ρ_0^e and ρ_f^e should be the same if there are no experimental errors. The colored band-region accounts for an artificial noise of the strength 5.79%, which is roughly estimated from the fitting error 3.00%, GRAPE imperfection error 1.59%, and decoherence error 1.20%. We added this noise on the theoretical state ρ_{AB}^0 , and randomly sampled 2500 states within the noise range for every λ (200 values in [0.1, 0.8]). The colored band-region is thus plotted based on the density of projected points out of 2500.

damping channel, which is of great importance in quantum information. By implementing this protocol, we show that given the experimental data collected for certain state ρ_{AB} , this protocol in fact leads to FST of ρ_{AB} . Therefore, this protocol does not lead to universal detection of entanglement of ρ_{AB} without FST.

Our study thus reveals a fundamental relationship between entanglement detection and quantum state tomography. That is, universal detection of entanglement without FST is impossible with only single-copy measurements. A natural question is what if joint measurements on r copies of the state ρ_{AB} (i.e. $\rho_{AB}^{\otimes r}$) for $r > 1$ are allowed. In this case, one indeed can detect entanglement universally for any ρ_{AB} without reconstructing the state, and one example for determining the concurrence of a two-qubit ρ_{AB} is given in [22–24]. However, the protocol of [23] involves joint measurements on 4 copies of ρ_{AB} (i.e. $\rho_{AB}^{\otimes 4}$), which makes the protocol hard to be implemented in practice. It will be interesting to find a smaller r such that joint measurements on c are enough to universally detect the entanglement in ρ_{AB} without full state tomography.

In fact, there are cases that this is possible even for $r = 2$. For instance we have found such a scheme that detects the entanglement of an arbitrary two-qubit state ρ_{AB} without FST, if we allow joint measurements on 2-copies. The idea is that ρ_{AB} is entangled if and only if [23] $\text{Det}(\rho_{AB}^T) < 0$,

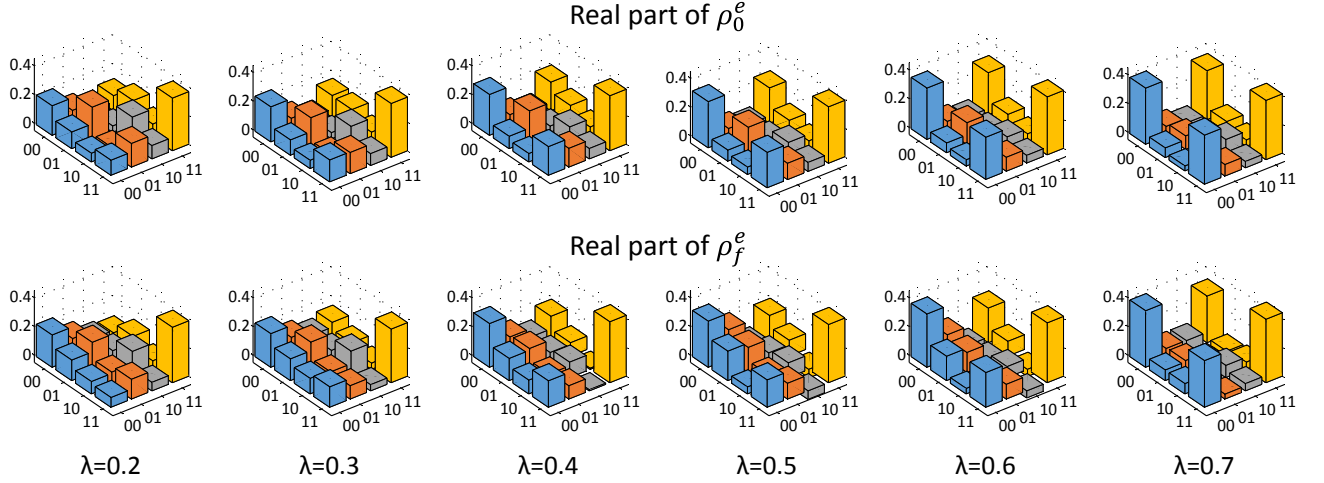


Figure 7. **Density matrices between ρ_0^e and ρ_f^e for different λ 's.** Only the real parts are displayed. The upper row shows the density matrices of ρ_0^e , which are obtained directly after the input state preparation via two-qubit state tomography. The lower row shows the density matrices of ρ_f^e , which are reconstructed through the single-qubit information after implementing the entire circuit in Fig. 2a. For any λ , the fidelity between ρ_0^e and ρ_f^e is always above 92%.

where ρ_{AB}^{TA} is the partial transpose of ρ_{AB} on system A . So we only need to design a scheme with measurements on $\rho_{AB}^{\otimes r}$ which can give the value of $\text{Det}(\rho_{AB}^{TA})$. This can indeed be done without FST (see supplemental materials for details).

Furthermore, if only single-copy measurements are allowed, one cannot determine the value of $\text{Det}(\rho_{AB}^{TA})$, even with adaptive measurements. Assume such adaptive measurements exist. Now, we let the input state is maximal mixed state $I/4$, after the measurement, one can compute the determinant. Notice that there exists at least one nonzero traceless R not measured, which means that this measurements can not distinguish between $I/4$ and $I/4 + tR$. Therefore, $\text{Det}(I/4 + tR^I) = \text{Det}(I/4)$ for sufficient small t . This then leads to $R = 0$.

This strongly supports our no-go results, which indicates that even with adaptive measurements, universal detection of entanglement with single-copy measurements is impossible without FST.

METHODS

Initialization in NMR. We first create the PPS from the thermal equilibrium state, which is a highly mixed state and not yet ready for quantum computation tasks. Since our sample consisting of four ^{13}C 's is a homonuclear system, we simply set the gyromagnetic ratio of ^{13}C to 1 and write the thermal equilibrium state as

$$\rho_{\text{thermal}} = \frac{I}{2^N} + \epsilon \sum_{i=1}^N \sigma_z^i, \quad (11)$$

where $N = 4$ is the number of qubits, I is the $2^N \times 2^N$ unity matrix, and $\epsilon \approx 10^{-5}$ represents the polarization at room temperature. This initialization step was realized by the spatial

average technique [42–44], and the related pulse sequence is depicted in Fig. 4. In particular, the gradient pulses represented by Gz crush all coherence in the instantaneous state. The final state after the entire PPS preparation sequence is

$$\rho_{0000} = \frac{1-\epsilon}{16} I + \epsilon |0000\rangle\langle 0000|. \quad (12)$$

It is worthy stressing that the large identity does not evolve under any unitary propagator, and it cannot be observed in NMR. Thus we only need to focus on the deviation part $|0000\rangle$ as the entire system behaves exactly the same as it does.

Our aim input state is ρ_{AB}^0 in equation (5). This mixed state consists of three components: $|\phi_B\rangle$, $|\phi_1\rangle$ and $|\phi_2\rangle$ with a weight for each. Typically we repeated every experiment by three times, and created one component in each round as the input. The sequences to prepare all three components are shown in the lower-right inset of Fig. 4, with all gates applied only on system qubits A and B. (i) For $|\phi_B\rangle$, we applied a Hadamard gate on qubit A, and then a controlled-NOT between A and B; (ii) for $|\phi_1\rangle$, we applied $R_x^A(\pi/2)$ and $R_y^B(\pi/2)$; (iii) for $|\phi_2\rangle$, we applied $R_y^A(\pi/2)$ and $R_x^B(0.7\pi)$. Subsequently, each component undergoes the whole filtering and measurement procedure respectively, with the final result obtained by summarizing over all three experiments.

Single-qubit tomography after each filter. The entanglement distillation procedure described in Ref. [33] involves iterative local filter operations, meaning that every filter depends on the single qubit measurement result before. In experiment we performed single-qubit tomography on system qubit C_2 or C_3 correspondingly. It requires the measurement of the expectation values of σ_x , σ_y and σ_z , respectively. In our 4-qubit system, this single-qubit tomography (assuming the measurement of C_3) is equivalent to measuring $|0\rangle\langle 0| \otimes \sigma_{x,y,z} \otimes I \otimes |0\rangle\langle 0|$, since we only need to focus in the subspace where the ancilla qubits are $|00\rangle$. To get the expectation values of the observables, a spectrum fitting procedure

was utilized to extract these results from NMR spectra. Supplementary Table S1 summarizes all of the single-qubit state fidelities and two-qubit state fidelities for every λ , and as an

example Supplementary Fig. S1 shows the NMR spectra after each filter to measure $\langle \sigma_x \rangle$ and $\langle \sigma_y \rangle$ of the current single qubit (C_2 or C_3) when $\lambda = 0.5$.

-
- [1] Einstein, A., Podolsky, B. & Rosen, N. Can quantum-mechanical description of physical reality be considered complete? *Phys. Rev.* **47**, 777 (1935).
- [2] Schrödinger, E. The present status of quantum mechanics. *Die Naturwissenschaften* **23**, 1–26 (1935).
- [3] Bell, J. S. *et al.* On the einstein-podolsky-rosen paradox. *Physics* **1**, 195–200 (1964).
- [4] Clauser, J. F. & Shimony, A. Bell’s theorem. experimental tests and implications. *Rep. Prog. Phys.* **41**, 1881 (1978).
- [5] Aspect, A., Grangier, P. & Roger, G. Experimental tests of realistic local theories via Bell’s theorem. *Phys. Rev. Lett.* **47**, 460 (1981).
- [6] Pan, J.-W., Bouwmeester, D., Daniell, M., Weinfurter, H. & Zeilinger, A. Experimental test of quantum nonlocality in three-photon Greenberger–Horne–Zeilinger entanglement. *Nature* **403**, 515–519 (2000).
- [7] Rowe, M. A. *et al.* Experimental violation of a Bell’s inequality with efficient detection. *Nature* **409**, 791–794 (2001).
- [8] Gröblacher, S. *et al.* An experimental test of non-local realism. *Nature* **446**, 871–875 (2007).
- [9] Ansmann, M. *et al.* Violation of Bell’s inequality in Josephson phase qubits. *Nature* **461**, 504–506 (2009).
- [10] Giustina, M. *et al.* Bell violation using entangled photons without the fair-sampling assumption. *Nature* **497**, 227–230 (2013).
- [11] Christensen, B. *et al.* Detection-loophole-free test of quantum nonlocality, and applications. *Phys. Rev. Lett.* **111**, 130406 (2013).
- [12] Hensen, B. *et al.* Loophole-free Bell inequality violation using electron spins separated by 1.3 kilometres. *Nature* **526**, 682–686 (2015).
- [13] Werner, R. F. Quantum states with Einstein-Podolsky-Rosen correlations admitting a hidden-variable model. *Phys. Rev. A* **40**, 4277 (1989).
- [14] Horodecki, R., Horodecki, P., Horodecki, M. & Horodecki, K. Quantum entanglement. *Rev. Mod. Phys.* **81**, 865–942 (2009).
- [15] Plenio, M. B. & Virmani, S. An introduction to entanglement measures. *Quantum Inf. Comput.* **7**, 1–51 (2007).
- [16] Cramer, M. *et al.* Efficient quantum state tomography. *Nat. Commun.* **1**, 149 (2010).
- [17] Hofheinz, M. *et al.* Synthesizing arbitrary quantum states in a superconducting resonator. *Nature* **459**, 546–549 (2009).
- [18] Jullien, T. *et al.* Quantum tomography of an electron. *Nature* **514**, 603–607 (2014).
- [19] Gühne, O. & Tóth, G. Entanglement detection. *Phys. Rep.* **474**, 1–75 (2009).
- [20] Mintert, F. Entanglement measures as physical observables. *Appl. Phys. B* **89**, 493–497 (2007).
- [21] Horodecki, P., Augusiak, R. & Demianowicz, M. General construction of noiseless networks detecting entanglement with the help of linear maps. *Phys. Rev. A* **74**, 052323 (2006).
- [22] Horodecki, P. Measuring quantum entanglement without prior state reconstruction. *Phys. Rev. Lett.* **90**, 167901 (2003).
- [23] Augusiak, R., Demianowicz, M. & Horodecki, P. Universal observable detecting all two-qubit entanglement and determinant-based separability tests. *Phys. Rev. A* **77**, 030301 (2008).
- [24] Bartkiewicz, K., Horodecki, P., Lemr, K., Miranowicz, A. & Życzkowski, K. Method for universal detection of two-photon polarization entanglement. *Phys. Rev. A* **91**, 032315 (2015).
- [25] Horodecki, P. & Ekert, A. Method for direct detection of quantum entanglement. *Phys. Rev. Lett.* **89**, 127902 (2002).
- [26] Carteret, H. A. Noiseless quantum circuits for the peres separability criterion. *Phys. Rev. Lett.* **94**, 040502 (2005).
- [27] Gühne, O., Reimpell, M. & Werner, R. Estimating entanglement measures in experiments. *Phys. Rev. Lett.* **98**, 110502 (2007).
- [28] Horodecki, P. From limits of quantum operations to multicopy entanglement witnesses and state-spectrum estimation. *Phys. Rev. A* **68**, 052101 (2003).
- [29] Bovino, F. A. *et al.* Direct measurement of nonlinear properties of bipartite quantum states. *Phys. Rev. Lett.* **95**, 240407 (2005).
- [30] Huber, M., Mintert, F., Gabriel, A. & Hiesmayr, B. C. Detection of high-dimensional genuine multipartite entanglement of mixed states. *Phys. Rev. Lett.* **104**, 210501 (2010).
- [31] Rudnicki, Ł., Horodecki, P. & Życzkowski, K. Collective uncertainty entanglement test. *Phys. Rev. Lett.* **107**, 150502 (2011).
- [32] Jungnitsch, B., Moroder, T. & Gühne, O. Taming multipartite entanglement. *Phys. Rev. Lett.* **106**, 190502 (2011).
- [33] Park, H. S., Lee, S. S. B., Kim, H., Choi, S. K. & Sim, H. S. Construction of an optimal witness for unknown two-qubit entanglement. *Phys. Rev. Lett.* **105**, 230404 (2010).
- [34] van Enk, S. J. & Beenakker, C. W. J. Measuring $\text{tr } \rho^n$ on single copies of ρ using random measurements. *Phys. Rev. Lett.* **108**, 110503 (2012).
- [35] Wootters, W. K. Entanglement of formation of an arbitrary state of two qubits. *Phys. Rev. Lett.* **80**, 2245 (1998).
- [36] Wang, Z.-W. *et al.* Experimental entanglement distillation of two-qubit mixed states under local operations. *Phys. Rev. Lett.* **96**, 220505 (2006).
- [37] Fisher, K. A., Prevedel, R., Kaltenbaek, R. & Resch, K. J. Optimal linear optical implementation of a single-qubit damping channel. *New J. Phys.* **14**, 033016 (2012).
- [38] Horodecki, M., Horodecki, P. & Horodecki, R. Separability of mixed states: Necessary and sufficient conditions. *Phys. Lett. A* **223**, 1–8 (1996).
- [39] Doherty, A. C., Parrilo, P. A. & Spedalieri, F. M. A complete family of separability criteria. *Phys. Rev. A* **69**, 022308 (2004).
- [40] Życzkowski, K., Horodecki, P., Sanpera, A. & Lewenstein, M. Volume of the set of separable states. *Phys. Rev. A* **58**, 883 (1998).
- [41] Verstraete, F., Dehaene, J. & De Moor, B. Normal forms and entanglement measures for multipartite quantum states. *Phys. Rev. A* **68**, 012103 (2003).
- [42] Cory, D. G., Fahmy, A. F. & Havel, T. F. Ensemble quantum computing by NMR spectroscopy. *Proc. Natl. Acad. Sci. U.S.A.* **94**, 1634–1639 (1997).
- [43] Lu, D. *et al.* Simulation of chemical isomerization reaction dynamics on a NMR quantum simulator. *Phys. Rev. Lett.* **107**, 020501 (2011).
- [44] Lu, D., Brodutch, A., Li, J., Li, H. & Laflamme, R. Experimental realization of post-selected weak measurements on an NMR quantum processor. *New J. Phys.* **16**, 053015 (2014).
- [45] Xin, T., Li, H., Wang, B.-X. & Long, G.-L. Realization of

- an entanglement-assisted quantum delayed-choice experiment. *Phys. Rev. A* **92**, 022126 (2015).
- [46] Khaneja, N., Reiss, T., Kehlet, C., Schulte-Herbrüggen, T. & Glaser, S. J. Optimal control of coupled spin dynamics: design of NMR pulse sequences by gradient ascent algorithms. *J. Magn. Reson.* **172**, 296–305 (2005).
- [47] Ryan, C., Negrevergne, C., Laforest, M., Knill, E. & Laflamme, R. Liquid-state nuclear magnetic resonance as a testbed for developing quantum control methods. *Phys. Rev. A* **78**, 012328 (2008).
- [48] Weinstein, Y. S. *et al.* Quantum process tomography of the quantum Fourier transform. *J. Chem. Phys.* **121** (2004).
- [49] Moussa, O., da Silva, M. P., Ryan, C. A. & Laflamme, R. Practical experimental certification of computational quantum gates using a twirling procedure. *Phys. Rev. Lett.* **109**, 070504 (2012).
- [50] Lu, D. *et al.* Experimental estimation of average fidelity of a Clifford gate on a 7-qubit quantum processor. *Phys. Rev. Lett.* **114**, 140505 (2015).
- [51] Carmeli, C., Heinosaari, T., Karlsson, A., Schultz, J. & Toigo, A. Verifying the quantumness of bipartite correlations. *arXiv:1510.03240* (2015).

Notes. After finishing this paper, we noticed a related recent work [51], where a similar idea of showing the set of separable states is not ‘cylinder-like’ is developed.

Author Contributions. D.L. and T.X. designed and carried out the NMR experiments and simulations; N.Y., Z.J., J.C. and B.Z. made the theoretical proposal and contributed to the analysis of results. X.P. and R.L. supervised the experiment. All authors contributed to the writing of the paper and discussed the experimental procedures and results.

Acknowledgments. We thank Y. Zhang for bringing the recent work [51] into our attention. We thank X. Ma for insightful discussions, and are grateful to the following funding sources: NSERC (D.L., N.Y., J.B., B.Z. and R.L.); Industry Canada (R.L.); CIFAR (B.Z. and R.L.); National Natural Science Foundation of China under Grants No. 11175094 and No. 91221205 (T.X. and G.L.), No. 11425523 and No. 11375167 (X.P.); National Basic Research Program of China under Grant No. 2015CB921002 (T.X. and G.L.).

Supplementary information: Tomography is necessary for universal entanglement detection with single-copy observables

Appendix A: A general method to show that the set of separable states is not ‘cylinder-like’.

We use two-qubit states as an example, however our method generalized naturally to the case of any bipartite systems (see supplemental materials for details).

Without loss of generality, we assume there is a set of S_i , where $1 \leq i \leq 14$, such that there is a function $g(\text{tr}(S_1\rho_{AB}), \text{tr}(S_2\rho_{AB}), \dots, \text{tr}(S_{14}\rho_{AB})) = 1$ for entangled ρ_{AB} , and 0 otherwise. One can hence view g as an analogue of an entanglement measure which is nonzero if and only if ρ_{AB} is entangled. Then one can find another observable R such that $\text{tr}R = 0$ and $\text{tr}(R^\dagger S_i) = 0$ for any $0 \leq i \leq 14$.

Our key observation is that for any non zero traceless R there exists some ρ_{AB} and real t such that $\rho_{AB} + tR$ is non-negative (hence is a quantum state), and ρ_{AB} is separable, $\rho_{AB} + tR$ is entangled. That is, $g(\rho_{AB})$ cannot exist.

To show this, we consider some state on the boundary of separable states, *i.e.*, the two-qubit isotropic states $\rho^{iso}(\alpha) = (1 - \alpha)I/4 + \alpha|\Phi\rangle\langle\Phi|$ with $|\Phi\rangle = \frac{1}{\sqrt{2}}(|00\rangle + |11\rangle)$ being the Bell state. It is known that the isotropic state $\rho^{iso}(\alpha)$ is separable if and only if $\alpha \geq 1/3$ [1, 2].

Now we let $\rho_{AB} = \rho^{iso}(\frac{1}{3}) = \frac{1}{6}I + \frac{1}{3}|\Phi\rangle\langle\Phi|$, so ρ_{AB} is separable. For any R , for sufficient small t , $\rho_{AB} + tR$ is non-negative since ρ_{AB} is positive(full rank). Choose $t > 0$ such that $\rho_{AB} + tR$ and $\rho_{AB} - tR$ are both non-negative. Therefore, $\rho_{AB} + tR$ and $\rho_{AB} - tR$ are separable. Notice that $\text{tr}(\sigma|\Phi\rangle\langle\Phi|) \leq 1/2$ holds for any separable state σ [3], we have

$$\begin{aligned} 1/2 &\geq \text{tr}[(\rho_{AB} + tR)|\Phi\rangle\langle\Phi|] \implies 0 \geq \text{tr}[R|\Phi\rangle\langle\Phi|], \\ 1/2 &\geq \text{tr}[(\rho_{AB} - tR)|\Phi\rangle\langle\Phi|] \implies 0 \leq \text{tr}[R|\Phi\rangle\langle\Phi|]. \end{aligned}$$

Thus, $\text{tr}[R|\Psi\rangle\langle\Psi|] = 0$ holds for arbitrary maximally entangled state $|\Psi\rangle = (U \otimes I)|\Phi\rangle$. In other words,

$$R = I \otimes M + N \otimes I,$$

with $\text{tr}(M) = \text{tr}(N) = 0$.

Notice that for any non-singular matrix S_A such that $S_A N S_A^\dagger$ is traceless, $R' = (S_A \otimes I)R(S_A \otimes I)^\dagger$ also satisfies the property that $\rho_{AB} + tR'$ is separable if and only if ρ_{AB} is separable and $\rho_{AB} + tR'$ is non-negative. According to the previous arguments, we know that R' can be written as $I \otimes M' + N' \otimes I$. Directly, one can conclude that $M = 0$. By choosing S_B such that $S_B N S_B^\dagger$ being traceless, we can obtain that $N = 0$. Therefore, R must be 0. In other words, tomography is required for detecting two-qubit entanglement by using the one copy non-adaptive measurement.

Appendix B: k -symmetric extension

In this section, we will show that the sets of states allowing k -symmetric extension are not ‘cylinder like’ for $k \geq 2$, even for two-qubit system, where a state ρ_{AB} is called k -symmetric extendable if and only if there exists $\sigma_{AB_1 B_2 \dots B_k}$ such that $\sigma_{AB_i} = \rho_{AB}$ for all $1 \leq i \leq k$.

We first recall that: A two-qudit Werner state is a state invariant under the $U \otimes U$ operator for all unitary U and has the following form

$$\rho_W(\psi^-) = \frac{1 + \psi^-}{2}\rho^+ + \frac{1 - \psi^-}{2}\rho^-,$$

where $\psi^- \in [-1, 1]$ is the parameter, ρ^+ and ρ^- are the states proportional to the projection of the symmetric subspace and anti-symmetric subspace respectively. $\rho_W(\psi^-)$ is k -symmetric extendable iff $\psi^- \geq -(d-1)/k$ proved in [4].

Assume that the set of states allowing k -symmetric extension is cylinder like. In other words there exists some traceless Hermitian operator R such that $\rho + tR$ is k -symmetric extendable if ρ is k -symmetric extendable and $\rho + tR$ is positive semidefinite.

Choose $\rho_0 = \rho_W(-(d-1)/k)$, then $\rho_0 > 0$ and for any R , there exists small t such that $\rho_0 + tR$ and $\rho_0 - tR$ are all positive semidefinite. Therefore, they are both k -symmetric extendable. As a direct consequence, we have Werner states σ_1 and σ_2 are

both k -symmetric extendable,

$$\begin{aligned}\sigma_1 &= \int_U (U \otimes U)(\rho_0 + tR)(U \otimes U)^\dagger dU \\ &= \rho_0 + t\text{tr}(RP^+)(\rho^+ - \rho^-), \\ \sigma_2 &= \int_U (U \otimes U)(\rho_0 - tR)(U \otimes U)^\dagger dU, \\ &= \rho_0 - t\text{tr}(RP^+)(\rho^+ - \rho^-),\end{aligned}$$

where P^+ and P^- are the projection onto the symmetric subspace and anti-symmetric subspace respectively.

By using condition of [4], one can conclude that

$$\begin{aligned}\frac{1 - (d-1)/k}{2} + t\text{tr}(RP^+) &\geq \frac{1 - (d-1)/k}{2}, \\ \frac{1 - (d-1)/k}{2} - t\text{tr}(RP^+) &\geq \frac{1 - (d-1)/k}{2}.\end{aligned}$$

Therefore,

$$\text{tr}(RP^+) = \text{tr}(R\rho^+) = \text{tr}(RP^-) = 0.$$

Similar technique can be applied for $(V \otimes I)\rho(V \otimes I)^\dagger$ with unitary V . That leads us to

$$\text{tr}(R(V \otimes I)\rho^+(V \otimes I)^\dagger) = 0.$$

That is, R^Γ , the partial transpose of R , is orthogonal to all maximally entangled state $(V \otimes I)|\Phi\rangle$,

$$\begin{aligned}&\text{tr}(R^\Gamma(V \otimes I)|\Phi\rangle\langle\Phi|(V \otimes I)^\dagger) \\ &= \text{tr}(R(V \otimes I)(P^+ - P^-)(V \otimes I)^\dagger) \\ &= 0.\end{aligned}$$

Now we write R as follows,

$$R_{AB}^\Gamma = I \otimes M + N \otimes I + X_{AB},$$

with $\text{tr}(M) = \text{tr}(N) = 0$, and $X_A = X_B = 0$. This can be done by simply choosing $M = \frac{(R_{AB}^\Gamma)_B}{d}$, $N = \frac{(R_{AB}^\Gamma)_A}{d}$ and $X_{AB} = R_{AB}^\Gamma - I \otimes \frac{(R_{AB}^\Gamma)_B}{d} - \frac{(R_{AB}^\Gamma)_A}{d} \otimes I$.

For sufficient small s , $I_{AB}/d + sX_{AB}$ is a choi matrix of some unital quantum channel. According to Theorem 1 of [5], we know that $I_{AB}/d + sX_{AB}$ is a linear combination of the density matrix of maximally entangled states, so is X_{AB} . Thus,

$$0 = \text{tr}(R_{AB}^\Gamma X_{AB}^\dagger) = \text{tr}(X_{AB} X_{AB}^\dagger),$$

where we use the fact that $I \otimes M + N \otimes I$ is orthogonal to all maximally entangled states. Thus, $X_{AB} = 0$ and R can be written as

$$R_{AB}^\Gamma = I \otimes M + N \otimes I.$$

Now, notice that for any non-singular matrix S_A such that $S_A N S_A^\dagger$ is traceless, $R' = (S_A \otimes I)R(S_A \otimes I)^\dagger$ also satisfies that $\rho_{AB} + tR'$ is k -symmetric extendable if and only if ρ_{AB} is k -symmetric extendable and $\rho_{AB} + tR'$ is non-negative. Then we know that R' can be written as $I \otimes M' + N' \otimes I$, too. Directly, one can conclude that $M = 0$. Thus, we only need to deal with

$$R = N^\Gamma \otimes I.$$

In the following, we deal with the two-qubit case. Note that there exists local unitary which transforms R into diagonal version $R = Z \otimes I = \text{diag}\{1, 1, -1, -1\}$.

We only construct some state ρ which is not 2-symmetric extendable [6] and $\rho + R$ is separable. Then such $\rho + R$ is k -symmetric extendable for all k while ρ is not 2-symmetric extendable.

$$\rho := \begin{pmatrix} x & 0 & 0 & \sqrt{xw} \\ 0 & y & \sqrt{yz} & 0 \\ 0 & \sqrt{yz} & z & 0 \\ \sqrt{xw} & 0 & 0 & w \end{pmatrix}, \quad (\text{B1})$$

$$\rho + R := \begin{pmatrix} x+1 & 0 & 0 & \sqrt{xw} \\ 0 & y+1 & \sqrt{yz} & 0 \\ 0 & \sqrt{yz} & z-1 & 0 \\ \sqrt{xw} & 0 & 0 & w-1 \end{pmatrix} \quad (\text{B2})$$

By using the condition of [6], ρ is not 2-symmetric extendable iff

$$\begin{aligned} (x+z)^2 + (y+w)^2 &< x^2 + y^2 + z^2 + w^2 + 2xw + 2yz, \\ \Leftrightarrow (x-y)(w-z) &> 0. \end{aligned}$$

$\rho + R$ is separable iff

$$\begin{aligned} (x+1)(w-1) &\geq xw, yz, \\ (y+1)(z-1) &\geq xw, yz. \end{aligned}$$

It is direct to see that one can choose some $w > z > x > y > 0$ such that

$$\begin{aligned} (x+1)(w-1) &\geq xw \geq yz, \\ (y+1)(z-1) &\geq xw \geq yz. \end{aligned}$$

Actually, we can choose ϵ to be sufficient small, and

$$\begin{aligned} x &= y + \epsilon, \\ z &= y + 2, \\ w &= y + 2 + \epsilon. \end{aligned}$$

Therefore, for all nonzero R , one can always find ρ and $\rho + R$ such that $\rho + R$ is separable and ρ is not 2-symmetric extendable. This shows that the set of states allowing k -symmetric extension is also not ‘cylinder-like’, even for two-qubit system.

Appendix C: The case of joint measurements

We discuss the case of joint measurements on r copies of ρ_{AB} (i.e. $\rho_{AB}^{\otimes r}$) with $r > 1$. We take the two-qubit case as an example. In this case, it is known that ρ_{AB} is entangled if and only if [7]

$$\text{Det}(\rho_{AB}^{T_A}) < 0, \quad (\text{C1})$$

where $\rho_{AB}^{T_A}$ is the partial transpose of ρ_{AB} on system A .

Notice that the determinant of $\rho_{AB}^{T_A}$ is a polynomial of degree 4 in terms of the matrix entries of ρ_{AB} , so it can be detected by measuring only a single observable on 4 copies of ρ_{AB} (i.e. $\rho_{AB}^{\otimes 4}$) [7].

For the case of joint measurements with $r = 2$, however, one cannot measure only a single observable to get $\text{Det}(\rho_{AB}^{T_A})$. Nevertheless, we show that the value of $\text{Det}(\rho_{AB}^{T_A})$ can be get without full state tomography with only a single joint measurement on $\rho_{AB}^{\otimes 2}$.

To see how this works, we rewrite $\rho_{AB}^{T_A}$ as

$$\rho_{AB}^{T_A} = \begin{pmatrix} R & S \\ S^\dagger & T \end{pmatrix},$$

with R is a 3×3 matrix, S is 3×1 , and T is 1×1 .

We can first determine R by single-copy measurements on $\rho_{AB}^{T_A}$, where 9 independent observables need to be measured. After that, T is known by the normalization condition $\text{tr}\rho_{AB}^{T_A} = 1$. This does not lead to a full state tomography on ρ_{AB} , since S is undetermined, with 6 free real parameters.

However, after knowing R and T , $\text{Det}(\rho_{AB}^{T_A})$ is a polynomial of degree 2 in terms of the matrix entries of ρ_{AB} , so it can be detected by measuring only a single observable on 2 copies of ρ_{AB} (i.e. $\rho_{AB}^{\otimes 2}$). Together with the measurements on R and S , we have total 10 measurement outcomes that determine universally whether ρ_{AB} is entangled or not. And this does not lead to full state tomography of ρ_{AB} , since ρ_{AB} needs 15 real parameters to determine.

In this way, we determine whether ρ_{AB} is entangled or not without full state tomography, by measuring a single observable on $\rho_{AB}^{\otimes 2}$ together with single copy measurements. This indicates that our no-go results for single copy measurements fail in the case if joint measurements are allowed, even for $r = 2$.

Appendix D: Experimental results of single-qubit tomography after each filter

Table S1 summarizes all of the single-qubit state fidelities and two-qubit state fidelities for every λ , and as an example Fig. S1 shows the NMR spectra after each filter to measure $\langle \sigma_x \rangle$ and $\langle \sigma_y \rangle$ of the current single qubit (C_2 or C_3) when $\lambda = 0.5$.

λ	Two-qubit Fidelity	Single-qubit Fidelity				
	$F(\rho_{AB}^0, \rho_0^e)$	Filter 1	Filter 2	Filter 3	Filter 4	Filter 5
0.2	0.9827	0.9987	0.9754	0.9691	0.9910	0.9698
0.3	0.9841	0.9994	0.9808	0.9984	0.9999	0.9916
0.4	0.9916	0.9995	0.9961	0.9942	0.9906	0.9865
0.5	0.9902	0.9989	0.9960	0.9960	0.9966	0.9969
0.6	0.9886	0.9996	0.9982	0.9982	0.9972	0.9965
0.7	0.9830	0.9983	0.9910	0.9997	0.9953	0.9955

Table S1. Fidelities of the experimental results compared with the theoretical ones for every λ . $F(\rho_{AB}^0, \rho_0^e)$ is the fidelity between the theoretical 2-qubit state ρ_{AB}^0 and ρ_0^e which is the truly prepared 2-qubit state. Meanwhile, the fidelities of the five single-qubit states after each filter are also shown.

-
- [1] Horodecki, M. & Horodecki, P. Reduction criterion of separability and limits for a class of protocols of entanglement distillation. *Phys. Rev. A* **59**, 4206–4216 (1999).
 - [2] Terhal, B. M. & Vollbrecht, K. G. H. The entanglement of formation for isotropic states. *Phys. Rev. Lett.* **85**, 2625–2628 (2000).
 - [3] Vidal, G. & Tarrach, R. Robustness of entanglement. *Phys. Rev. A* **59**, 141–155 (1999).
 - [4] Johnson, P. D. & Viola, L. Compatible quantum correlations: Extension problems for werner and isotropic states. *Phys. Rev. A* **88**, 032323 (2013).
 - [5] Mendl, C. B. & Wolf, M. M. Unital quantum channels - convex structure and revivals of Birkhoff's theorem. *Commun. Math. Phys.* **289**, 1057–1096 (2009).
 - [6] Chen, J., Ji, Z., Kribs, D., Lutkenhaus, N. & Zeng, B. Symmetric extension of two-qubit states. *Phys. Rev. A* **90**, 032318 (2014).
 - [7] Augusiak, R., Demianowicz, M. & Horodecki, P. Universal observable detecting all two-qubit entanglement and determinant-based separability tests. *Phys. Rev. A* **77**, 030301 (2008).

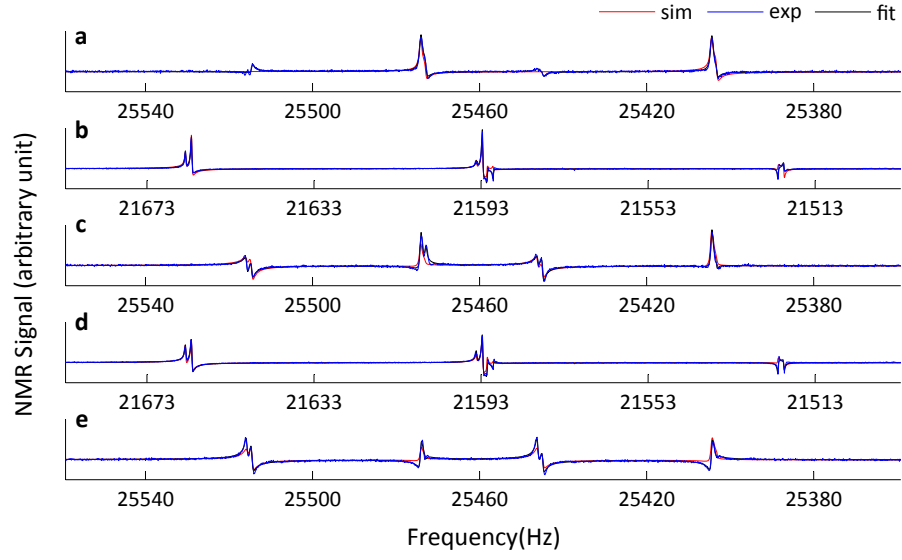


Figure S1. NMR spectra of measuring $\langle \sigma_x \rangle$ and $\langle \sigma_y \rangle$ of single qubit after each filter for $\lambda = 0.5$. (a-e) are produced after filter 1-5, respectively. (a, c, e) show spectra of C_2 , and (b, d) show C_3 . The red curve is the simulation result assuming the input state is $|0\rangle\langle 0| \otimes \rho_0^e \otimes |0\rangle\langle 0|$, and the blue curve is the experimental result which can be used to extract $\langle \sigma_x \rangle$ and $\langle \sigma_y \rangle$ of the current qubit. The black curve shows the fitting spectrum to obtain $\langle \sigma_x \rangle$ and $\langle \sigma_y \rangle$. To measure $\langle \sigma_z \rangle$, we rotated it to σ_x with a $\pi/2$ pulse around y -axis and then measured. It can be seen that the fitting matches extremely well with the experimental result, which means our readout values are very accurate.